SCIENTIFIC REPORTS

OPEN

Theoretical predictions on the electronic structure and charge carrier mobility in 2D Phosphorus sheets

Received: 11 January 2015
Accepted: 25 March 2015
Published: 02 June 2015

Jin Xiao[1], Mengqiu Long[1,2], Xiaojiao Zhang[1], Jun Ouyang[1], Hui Xu[1] & Yongli Gao[1,3]

We have investigated the electronic structure and carrier mobility of four types of phosphorous monolayer sheet (α-P, β-P,γ-P and δ-P) using density functional theory combined with Boltzmann transport method and relaxation time approximation. It is shown that α-P, β-P and γ-P are indirect gap semiconductors, while δ-P is a direct one. All four sheets have ultrahigh carrier mobility and show anisotropy in-plane. The highest mobility value is ~3×10^5 $cm^2V^{-1}s^{-1}$, which is comparable to that of graphene. Because of the huge difference between the hole and electron mobilities, α-P, γ-P and δ-P sheets can be considered as *n*-type semiconductors, and β-P sheet can be considered as a *p*-type semiconductor. Our results suggest that phosphorous monolayer sheets can be considered as a new type of two dimensional materials for applications in optoelectronics and nanoelectronic devices.

Since the successful preparation of graphene[1], two-dimensional(2D) atomically-thick materials, such as graphdiyne sheet[2], boron nitride sheet[3], silicene[4] and layered transition-metal dichalcogenides[5,6] have attracted intensive attention owing to their unique physical properties and potential applications in nanoscale devices. Recently, due to the synthesis of few layers black phosphorus (BP)[7–10], named phosphorene, 2D phosphorous materials have become the focus of science community[11–22]. BP is the most stable phosphorus allotrope under normal conditions with a direct band gap of about 0.3 eV[23–25]. The direct band gap will increase to ~2.0 eV[26,27] as BP reduces to a monolayer, which opens doors for applications in optoelectronics. Furthermore, bulk BP is found to have high carrier mobility in the order of 10^5 $cm^2V^{-1}s^{-1}$ at low temperatures[28,29]. The field-effect carrier mobility of few-layer BP is measured to be still higher, up to 1000 $cm^2V^{-1}s^{-1}$ for electron[7] and 286 $cm^2V^{-1}s^{-1}$ for hole[8] at room temperature. Also, few-layer BP exhibits ambipolar behavior with drain current modulation up to 10^5[7]. Owing to the direct gap and high mobility, there is a high potential for BP thin crystals to be a new 2D material for applications in optoelectronics, nanoelectronic devices and so on[30–36].

So far, there have been few reports about the mobility of monolayer BP experiment researches. Theory studies based on effective mass calculation[25] have shown that the room temperature electron mobility of monolayer BP is over 2000 $cm^2V^{-1}s^{-111}$ or 5000 $cm^2V^{-1}s^{-119}$. However, the method is subject to the parabolic properties of the energy bands. In this paper, both of electron and hole mobilities are investigated with Boltzmann transport equation (BTE) method beyond the effective mass approximation. Furthermore, besides the monolayer BP (marked as α-P), other three stable 2D phosphorus allotropes, namely β-P, γ-P and δ-P based on theoretical predictions[20,21], have also been investigated. We therefore report the first theoretical prediction on the charge mobility of those 2D phosphorus allotropes in this work.

[1]Institute of Super-microstructure and Ultrafast Process in Advanced Materials, School of Physics and Electronics, Central South University, Changsha 410083, China. [2]Department of Physics and Materials Science, City University of Hong Kong, Hong Kong, China. [3]Department of Physics and Astronomy, University of Rochester, Rochester, NY 14627, USA. Correspondence and requests for materials should be addressed to M.L. (email: mqlong@csu.edu.cn) or H.X. (email: cmpxhg@csu.edu.cn)

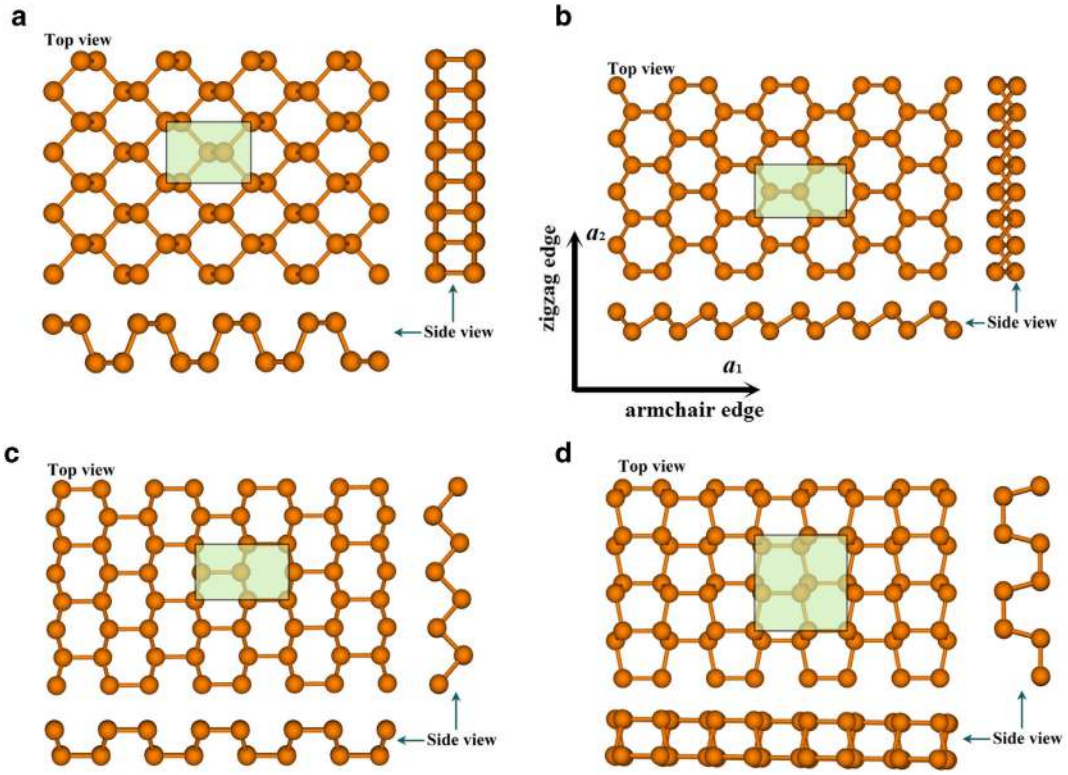

Figure 1. The models of phosphorus sheets: (**a**) α-P, (**b**) β-P, (**c**) γ-P and (**d**) δ-P.

	Lattice length (Å)		*d* (Å)	Energy (eV/atom)	P-bond length (Å)
	armchair	zigzag			
α-P	4.626 4.53[a]	3.298 3.36[a]	2.103	-5.364	2.233
β-P	5.677 5.77[a]	3.278 3.33[a]	1.237	-5.363	2.261
γ-P	5.420 5.34[a]	3.268 3.41[a]	1.492	-5.272	2.271
δ-P	5.416 5.46[a]	5.531 5.56[a]	2.141	-5.287	2.256

Table 1. The lattice length, distance of two P atom sub-layers (*d*), the energy per atom and average P-bond length in phosphorus sheets. [a]Theory results from Ref. 21.

Results

The atomic structures of four different types of phosphorus sheets are shown in Fig. 1. In order to get an intuitive demonstration of carrier conduction along the armchair and zigzag directions, an orthogonal supercell covered by a green shadow is used in Fig. 1. The lattice length is shown in Table 1, and is in agreement with previous studies. There are four phosphorus (P) atoms in the supercell of α, β,

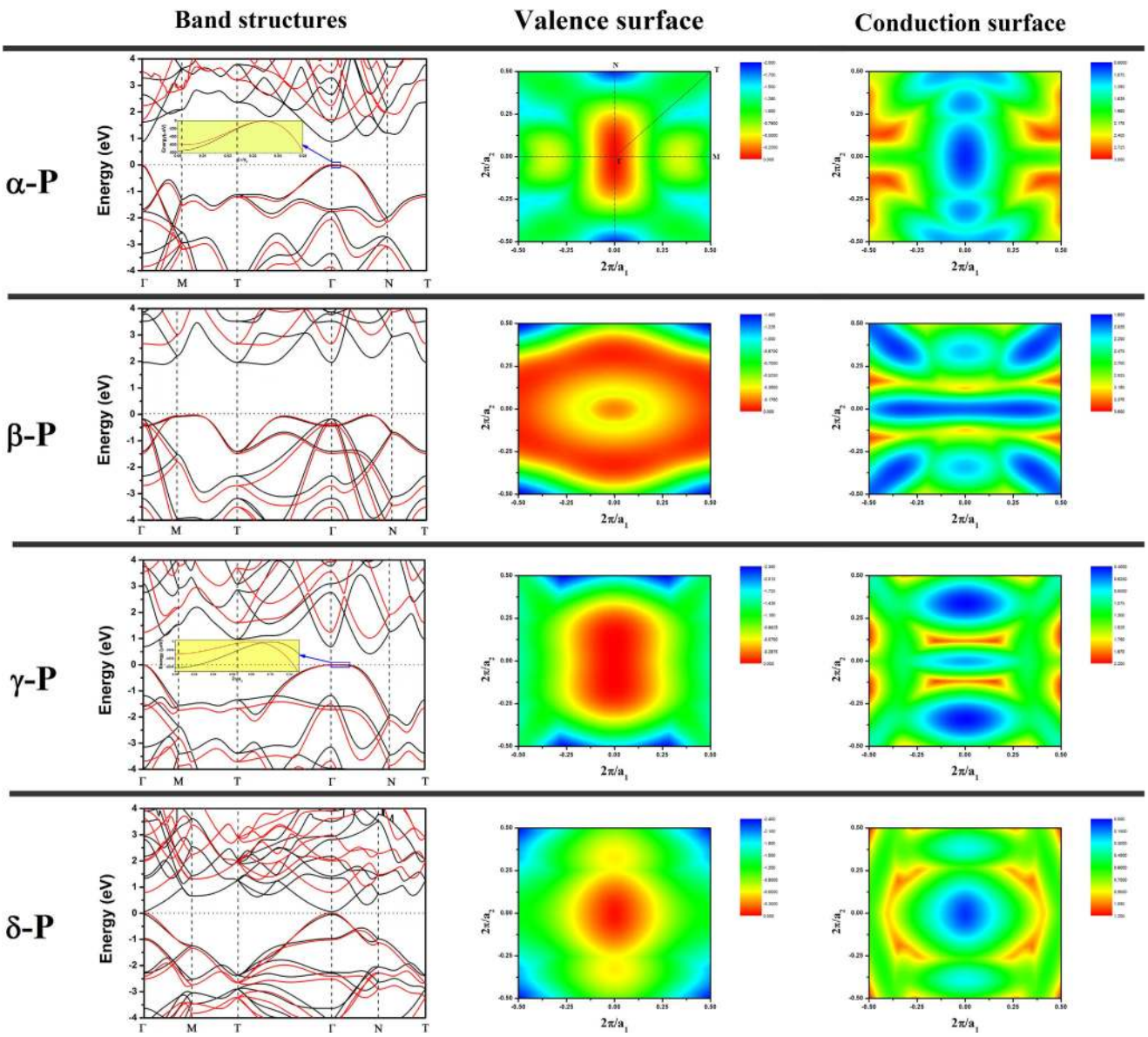

Figure 2. Energy band structures, valance band edge surface heat map and conduction band edge surface heat map of α-P, β-P, γ-P and δ-P. Red arrows are the direct gaps at Γ point. The black lines and red lines in band structures are calculated by PBE and HSE06 respectively. K point: Γ(0,0,0), M(0.5, 0, 0), N (0, 0.5, 0), T(0.5, 0.5, 0).

γ phosphorus (α-P, β-P, γ-P), and eight P atoms in the supercell of δ phosphorus (δ-P). There are two phosphorus sub-layers in each phosphorus sheet. The distance of two P sub-layers (d) is shown in Table 1. The energy per atom indicates that α-P sheet is the most stable. The average P bond length is about 2.23 ~ 2.27 Å.

Energy band structures and Fermi surface heat map of the phosphorus sheets are shown in Fig. 2. All four types of phosphorus sheets are semiconductors. For α-P, β-P, γ-P and δ-P, as shown in Table 2, the energy band gaps based on PBE (HSE06) calculation are 0.91(1.70), 1.93(2.64), 0.42(1.03) and 0.10(0.78) eV, respectively. The energy band structures and band gaps are consistent to those reported in previous studies[21]. Our calculations indicate that only δ-P is a direct gap semiconductor. The other three type sheets are indirect semiconductors. These results are in good agreement with previous study[20,21]. Interestingly, when we zoom in the energy band spectrum around the Γ point in α-P, as shown in the inset of Fig. 2 we can find that the top of the valence band is located at (0, 0.035) K point (skewed slightly along the zigzag direction) and is about 0.75 (0.53) meV higher than the Γ point based on the PBE (HSE06) calculation. This tiny skewing away Γ point on the top of the valence band is in good

Energy gap (eV)	α-P	β-P	γ-P	δ-P
Direct gap (Γ point)	0.9093[a]	2.1427[a]	0.6958[a]	0.1034[a]
	1.7014[b]	3.0028[b]	1.2516[b]	0.7839[b]
Indirect gap	0.9085[a]	1.9341[a]	0.4232[a]	-
	1.7009[b]	2.6399[b]	1.0301[b]	

Table 2. The energy gap of phosphorus sheets: [a]is the PBE results; [b]is the HSE06 results.

agreement with Ref. 37 and has also been demonstrated in α-P zigzag nanoribbon[16]. The optical characteristics should be influenced only slightly in α-P sheets due to such tiny skewing.

Based on the band structures, we calculate the effective mass of the charge carrier by parabolic fitting near the Fermi surface, which is presented in Table 3. It can be found that most of $|m^*|$ is smaller than the mass of the free electron (m_e), which means that the phosphorus sheets have considerably high carrier mobility. Our results show that the m^* for electrons and holes in α-P are 0.1382 and 1.2366 m_e, respectively, which are in good agreement with *Yang's* report[11]. Furthermore, it is clearly seen that the $|m^*|$ of electron or hole along the armchair direction over an order of magnitude smaller than that along the zigzag direction. It indicates that the carrier transport is anisotropic and the armchair direction is the main transport direction in α-P. The case in β-P is the opposite. The $|m^*|$of electron or hole along the zigzag direction is three times larger than that along the armchair direction, which means that the carrier transport ability is stronger along the armchair than the zigzag direction in β-P. It is easily to see that the $|m^*|$ of hole along the zigzag direction in α-P and γ-P is much larger than others', which result from the almost flat valence band in those materials.

The variation of total energy (E) with uniaxial strain (δ) applied along the armchair and zigzag directions are shown in Fig. 3. Based on those energy-strain curves, the in-plane stretching modulus C^{2D} can be obtained. In α-P sheets, we can also find that C^{2D} is obvious anisotropic, and it is about four times larger along the zigzag direction (103.278 N/m) than along the armchair direction (24.255 N/m). These are in good agreement with *Qiao*'s report (101.60 and 28.94 N/m)[25]. In general, the three-dimensional Young's modulus can be estimated as $C^{3D} = C^{2D}/t_0$. Based on the optB86b van der Waals functional, the interlayer separation of α-P, β-P, γ-P and δ-P have been calculated as 5.30, 4.20, 4.21 and 5.47 Å[21], respectively. By assuming a finite thickness (t_0 = 5.30, 4.20, 4.21 and 5.47 Å) for α-P, β-P, γ-P and δ-P sheet, the Young's modulus along the armchair and zigzag direction are shown in Table 4. The previous theoretical study has shown the Young's modulus of monolayer α-P sheet to be 44 GPa (armchair direction) and 166 GPa (zigzag direction)[31].

Figure 4 shows the shifts of band edges as a function of strain along the armchair and zigzag directions. Through dilating the lattice along the armchair and zigzag directions, the DP constant E_1 is then calculated as $dE_{edge}/d\delta$, equivalent to the slope of the fitting lines, where E_{edge} is the energy of the conduction (valence) band edge. Each line is fitted by 11 points. The E_1 values of phosphorus sheets are shown in Table 5. The standard error of all E_1 values is smaller than 1% excluding three valuses marked in Table 5.

$m^*(m_e)$	Direction	α-P	β-P	γ-P	δ-P
electron	Armchair	0.1382	0.9416	0.4831	0.1218
	Zigzag	1.2366	0.1356	0.3680	0.3871
hole	Armchair	-0.1315	-3.4754	-0.4150	-0.1099
	Zigzag	-6.1693	-0.8347	-5.7610	-0.4118

Table 3. The effective mass (m^*) of carriers in phosphorus sheets.

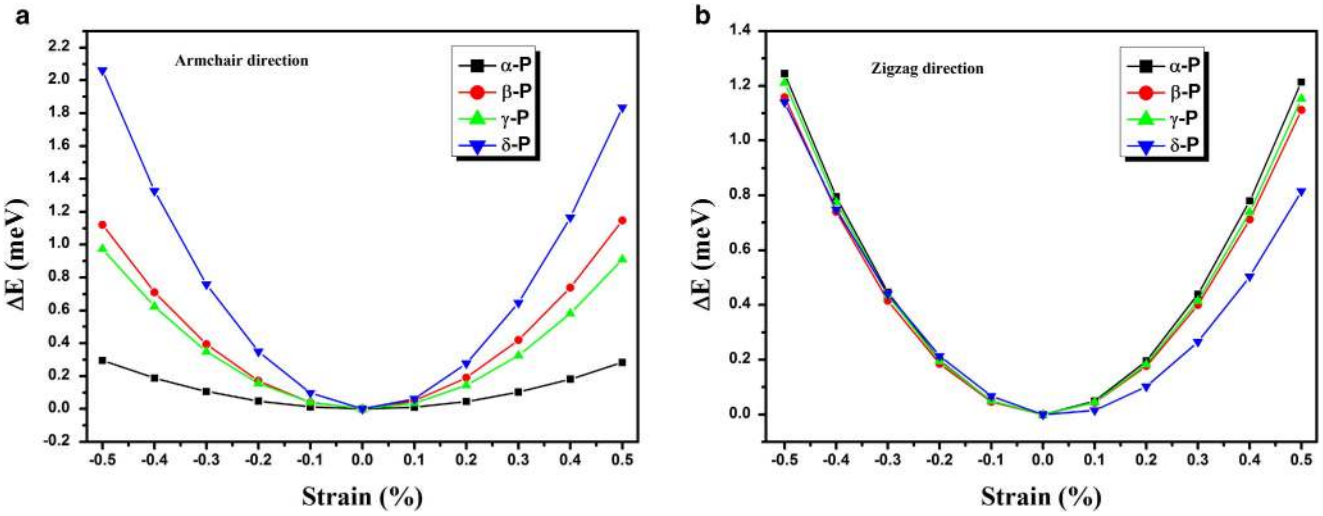

Figure 3. Energy−strain relationship along armchair (**a**) and zigzag (**b**) directions.

On the basis of our energy band spectrum, we calculated E_1 and C^{2D}, the acoustic phonon-limited mobility (using Eq. 1) and relaxation time (using Eq. 2) at room temperature (300 K). The results are shown in Table 5. It can be seen that the electron relaxation time (τ_e) in phosphorus sheets is much longer than the hole relaxation time (τ_h), excluding β-P. The electron mobilities of α-P, β-P, γ-P and δ-P sheets are about 1.1×10^4, 4.7×10^2, 2.9×10^5 and 3.0×10^3 $cm^2V^{-1}s^{-1}$, respectively. The corresponding τ_e's are about 1.29, 0.09, 70.73 and 0.61 ps. The hole mobilities of α-P, β-P, γ-P and δ-P sheets are about 2.0×10^2, 1.7×10^3, 7.3×10^1 and 5.9×10^2 $cm^2V^{-1}s^{-1}$, respectively. The corresponding τ_h's are about 0.02, 0.86, 0.24 and 0.09 ps. It can be found that all four phases have higher mobility than MoS_2 monolayer sheet (the hole mobility is 86 $cm^2V^{-1}s^{-1}$ and electron mobility is 44 $cm^2V^{-1}s^{-1}$)[38]. Due to the very small conduction band deformation potential (0.187 eV), the electron mobility along the zigzag direction in γ-P sheet is as high as ~3×10^5 cm^2/Vs, which is in the same order of magnitude of that in graphene[42,47], silicone[39] and germanene[40]. The minimum is the electron mobility along the zigzag direction in β-P sheet, which is about 47.32 cm^2/Vs. The electron carriers move faster than the hole ones in α-P, γ-P and δ-P sheet. Only in β-P sheet, the hole mobility is higher than the electron mobility. γ-P sheet has the best electron carrier transmitting capacity and the biggest difference between the electron and hole mobility in four type sheets. Moreover, the obvious anisotropy in carrier mobility can be found. The charge carriers move faster along the armchair direction than the zigzag direction in α-P, β-P and δ-P sheet. While in γ-P sheet, the zigzag direction is preferred.

Discussion

It must be noted that the mobility in our calculation is a theoretical value. Only the acoustic phonon scattering mechanism is considered. Actually, there are inevitably impurities and defects in the vast majority of materials, and they have a great influence on the charge transport properties, especially at

	Armchair direction (GPa)	Zigzag direction(GPa)
α-P	45.76	194.86
β-P	185.92	186.18
γ-P	167.83	203.25
δ-P	152.18	76.34

Table 4. Three-dimensional Young's modulus (C^{3D}) of phosphorus sheets.

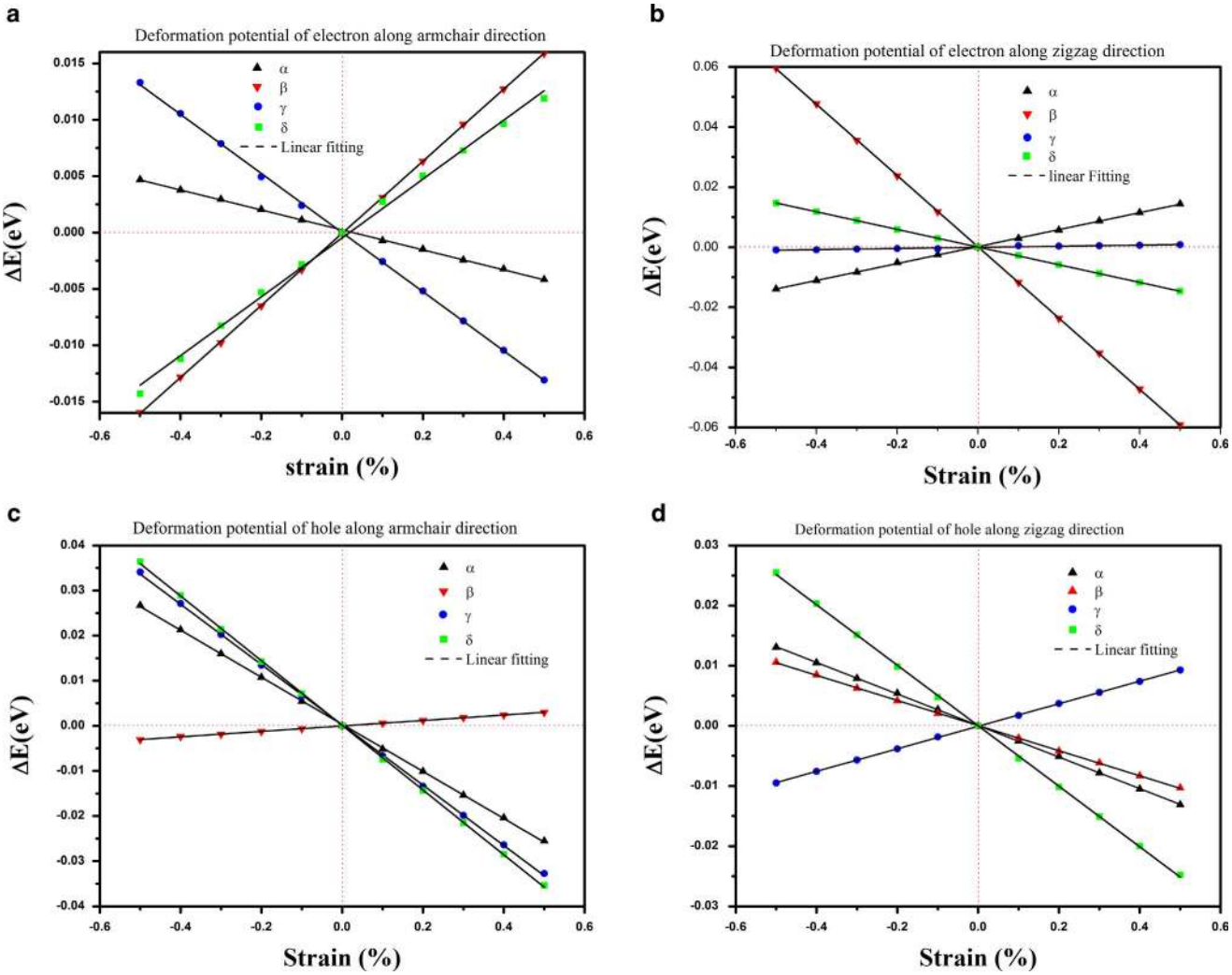

Figure 4. Shifts of conduction band and valence band under uniaxial strain: conduction band along (**a**) armchair and (**b**) zigzag direction; valence band along (**c**) armchair and (**d**) zigzag direction. The balck dashed line is the linear fitting.

low temperatures where phonon has little effect[47]. For example, in a MoS_2 sheet, owing to scattering from charged impurities, the mobility at low-temperatures signally decreases with temperature[41]. So the mobility of phosphorus sheets measured experimentally can be much smaller than theoretically predicted.

The band decomposed charge density around the Fermi level of phosphorus sheets is shown in Fig. 5. The composition of the top valence and the bottom conduction band are shown in Table 6. Atomic orbital analysis shows that the top of valence states in phosphorus sheets are mainly composed of $3p_z$ orbits. Our calculations indicate that, in α-P, the conduction bands are mainly composed of p_z orbitals with mixed s and p_x orbits. In β-P, the conduction bands are hybridization orbitals with mixed s and p orbits. In γ-P, the conduction bands are mainly composed of p_y and p_z orbitals. In δ-P, the conduction bands are major composed of p_z and s orbitals.

In α-P, β-P and γ-P, owing to the valence bands partly composed of in-plane p orbits, the top of the valence band is skewing awaly the Γ point. Due to the distribution of the mainly charge density of the valence is along the armchair direction, the hole carrier will move faster along the armchair direction than the zigzag direction in α-P, β-P and δ-P. While in γ-P, due to the contributions of s and p_z orbitals, the distribution of valence band charge density is along the zigzag direction (Fig. 5c). So the hole mobility in γ-P is slightly higher along the zigzag direction than the armchair direction. For the conduction band, the distribution of charge density is along the armchair direction, as shown in Fig. 5e,f, and g. This is identical with the electron mobility except γ-P. The orbital analysis shows that the proportion of p_x orbital is larger than that of p_y orbit except γ-P and δ-P. Due to the contribution of p_x orbitals, the electron mobility is higher along the armchair direction than the zigzag direction in α-P and β-P. In γ-P,

	direction	C^{2D} (Nm^{-1})	E_1 of electron(eV)	$E_1$of hole (eV)	τ_e(ps)	τ_h(ps)	μ_e (cm^2/Vs)	μ_h (cm^2/Vs)
α-P	armchair	24.255	-0.886[a]	-5.222	1.2896	0.0217	1.107×10^4	2.043×10^2
	zigzag	103.278	2.821	-2.624	0.5416	0.3666	6.035×10^2	1.495×10^2
β-P	armchair	78.088	3.198	0.605	0.0944	0.8577	4.663×10^2	1.711×10^3
	zigzag	78.194	-11.853	-2.090	0.0069	0.0720	4.732×10^1	6.426×10^1
γ-P	armchair	68.130	-2.622[b]	-6.687	0.2879	0.0148	1.482×10^3	5.711×10^1
	zigzag	85.569	0.187[c]	1.875	70.9731	0.2360	2.895×10^5	7.264×10^1
δ-P	armchair	83.245	2.611	-7.173	0.6077	0.0910	3.022×10^3	5.863×10^2
	zigzag	41.760	-2.938	-5.031	0.2409	0.0927	7.790×10^2	2.830×10^2

Table 5. The in-plane elastic constant (C^{2D}), deformation potential (E_1), electron relaxation time (τ_e), hole relaxation time (τ_h), electron mobility (μ_e) and hole mobility (μ_h) in phosphorus sheets. The temperature is 300K.The Standard Error is [a]1.01%, [b]1.78%, [c]8.06% and others smaller than 1%.

the contribution of p_y orbits is over 50%. At the same time, there is much lower deformation potential. So the electron mobility along zigzag is surperisely high in γ-P.

Conclusions

In summarily, we have calculated the electronic structures and the intrinsic charge carrier mobility of four type phosphorus sheets (α-P, β-P, γ-P and δ-P), using first-principles density functional theory and the BTE with the relaxation time approximation. We find that α-P, β-P and γ-P are indirect gap semiconductors. The numerical results indicate that the electron mobility of α-P, γ-P and δ-P sheets at room temperature (about 1.107×10^4, 2.895×10^5 and $3.022\times10^3\,cm^2V^{-1}s^{-1}$, respectively) is much higher thanthe corresponding hole mobility (about 204.288, 72.645 and $586.339\,cm^2V^{-1}s^{-1}$, respectively). Nevertheless, in β-P sheet, the hole mobility ($1.711\times10^3\,cm^2V^{-1}s^{-1}$) is about four times of electron

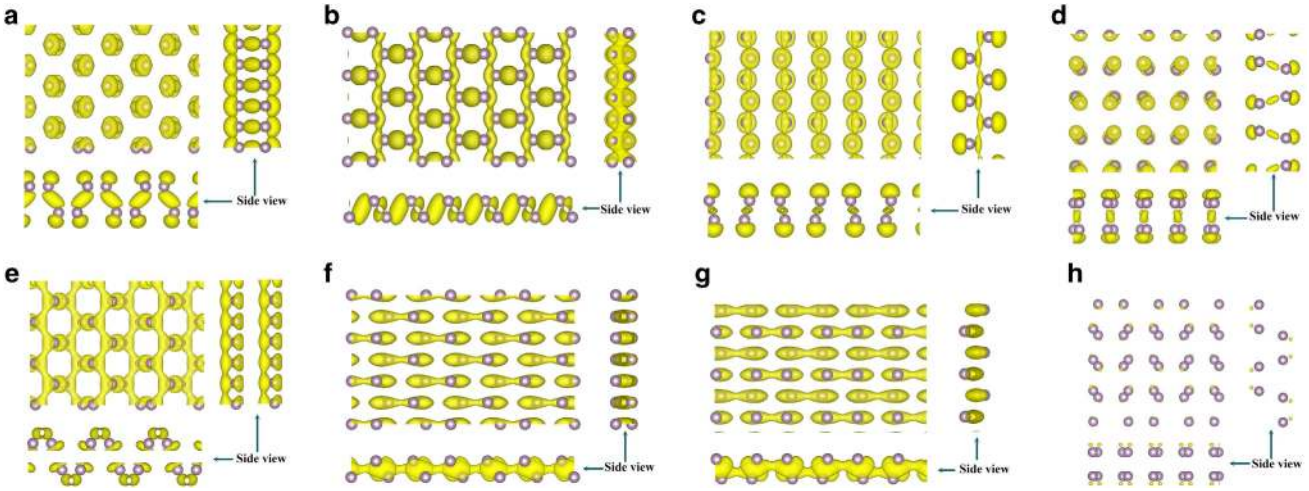

Figure 5. Band decomposed charge density of phosphorus sheets: (**a**)–(**d**) is the valance band edge for α-P, β-P, γ-P and δ-P respectively; (**e**)–(**h**) is the conduction band edge for α-P, β-P, γ-P and δ-P respectively. The isosurface value is 0.01. Drawings are produced by VESTA software[42].

		s	p_y	p_z	p_x
α-P	valance	7.210	0.067	89.928	2.795
	conduction	14.023	0.002	65.648	20.327
β-P	valance	8.453	3.502	82.521	5.524
	conduction	28.346	14.908	38.264	18.482
γ-P	valance	8.4841	1.241	90.255	0.020
	conduction	9.549	56.419	27.993	6.039
δ-P	valance	15.002	0.435	84.355	0.209
	conduction	14.360	7.903	70.254	7.484

Table 6. The percentage (%) of each orbit in the top of valance and the bottom of conduction.

mobility (466.262 $cm^2V^{-1}s^{-1}$). Owing to the huge difference mobilities in hole and electron, α-P, γ-P and δ-P sheets can be considered as *n*-type semiconductors, and β-P sheet can be considered as *p*-type semiconductors. All four types of phosphorus sheets present anisotropy in carrier mobility. Charge carriers move faster along the armchair direction than the zigzag direction in α-P, β-P and δ-P sheet. But in γ-P sheet, the more favorable charge transmission direction is along zigzag.

Methods

In this paper, the carrier mobility is calculated by BTE method beyond the effective mass approximation which is used to predict the mobility of semiconductor nanometerials, like graphene, carbon nanotubes and so on[2,43–48]. Within the BTE method, the carrier mobility μ in the relaxation time approximation can be express as Ref. 2 and 49:

$$\mu^{e(h)} = \frac{e}{k_B T} \frac{\sum_{i\in CB(VB)} \int \tau(i, \vec{k}) v^2(i, \vec{k}) \exp\left[\mp \frac{\varepsilon_i(\vec{k})}{k_B T}\right] d\vec{k}}{\sum_{i\in CB(VB)} \int \exp\left[\mp \frac{\varepsilon_i(\vec{k})}{k_B T}\right] d\vec{k}} \quad (1)$$

Where the minus (plus) sign is for electron (hole). $\tau(i, \vec{k})$ is the relaxation time, $\varepsilon_i(\vec{k})$ and $v(i, \vec{k})$ are band energy and the component of group velocity at $\vec{k}$ state of the *i*-th band, respectively. The summation of band was carried out over VB for hole and CB for electron. Furthermore, the integral of $\vec{k}$ states is over the first Brillouin zone (BZ).

In order to obtain the mobility, three key quantities ($\tau(i, \vec{k})$, $\varepsilon_i(\vec{k})$ and $v(i, \vec{k})$) must be determined. The coherent wavelength of thermally activated electrons or holes at room temperature in inorganic semiconductors, which is much larger than their lattice constant, is close to that of acoustic phonon modes in the center of the first BZ. The electron−acoustic phonon coupling can be effectively calculated by the deformation potential (DP) theory proposed by Bardeen and Shockley[50]. So, the relaxation time $\tau(i, \vec{k})$ based on DP theory can be expressed as[2,48]

$$\frac{1}{\tau(i, \vec{k})} = k_B T \frac{2\pi E_1^2}{\hbar C} \sum_{k'\in BZ} \left\{ \left[1 - \frac{\vec{v}\left(i, \vec{k'}\right)}{\vec{v}(i, \vec{k})} \right] \delta\left[\varepsilon(\vec{k}) - \varepsilon\left(\vec{k'}\right) \right] \right\} \quad (2)$$

Here the delta function denotes that the scattering process is elastic and occurs between the band states with the same band index. $E_1$is the DP constant of the *i*-th band, and *C* is the elastic constant.

The band energy $\varepsilon_i(\overrightarrow{k})$ is calculated by the Vienna *ab-initio* simulation package (VASP)[51]. The $\overrightarrow{k}$ -mesh is chosen as $11 \times 11 \times 1$ for electronic structures calculation and $61 \times 61 \times 1$ for band eigenvalue calculation, which is fine enough to give converged relaxation time and mobility. The generalized gradient approximation (GGA)[52] with the Perdew-Burke-Ernzerhof (PBE)[53] exchange correlation function is used with the plane-wave cutoff energy set at 600 eV for all calculations. The criterion of convergence is that the residual forces are less than 0.001 eV/Å and the change of the total energy is less than 10^{-7} eV. The vacuum space between two adjacent sheets is set at least 15 Å to eliminate the interactive effect on each other.

The group velocity of electron and hole carriers can be obtained from the gradient of the band energy $\varepsilon_i(\overrightarrow{k})$ in $\overrightarrow{k}$-space, $v(i, \overrightarrow{k}) = \nabla\varepsilon_i(\overrightarrow{k})/\hbar$.

References

1. Geim, A. K. & Novoselov, K. S. The rise of graphene. *Nat. mater.* **6,** 183–191 (2007).
2. Long, M. *et al.* Electronic Structure and Carrier Mobility in Graphdiyne Sheet and Nanoribbons: Theoretical Predictions. *ACS Nano* **5,** 2593–2600 (2011).
3. Levendorf, M. P. *et al.* Graphene and boron nitride lateral heterostructures for atomically thin circuitry. *Nature* **488,** 627–632 (2012).
4. Tahir, M. & Schwingenschlogl, U. Valley polarized quantum Hall effect and topological insulator phase transitions in silicene. *Sci. Rep.* **3,** 1075 (2013).
5. Wang, Q. H.*et al.* Electronics and optoelectronics of two-dimensional transition metal dichalcogenides. *Nat. Nanotech.* **7,** 699–712(2012).
6. Xiao, J. *et al.* Effects of Van der Waals interaction and electric field on the electronic structure of bilayer MoS_2. *J. Phys.: Condens. Matter* **26,** 405302 (2014).
7. Li, L. *et al.* Black phosphorus field-effect transistors. *Nat. Nanotech.* **9,** 372 (2014).
8. Liu, H. *et al.* Phosphorous: An Unexplored 2D Semiconductor with a High Hole Mobility. *ACS Nano*. **8,** 4033 (2014).
9. Köpf, M. *et al.* Access and *in situ* growth of phosphorous-precursor black phosphorus. *J. Cryst. Growth* **405,** 6–10 (2014).
10. Lu, W. *et al.* Plasma-assisted fabrication of monolayer phosphorous and its Raman characterization. *Nano Res.* **7,** 853–859 (2014).
11. Fei R. & Yang, L. Strain-Engineering the Anisotropic Electrical Conductance of Few-Layer Black Phosphorus. *Nano Lett.* **14,** 2884−2889 (2014).
12. Han, X. *et al.* Strain and Orientation Modulated Bandgaps and Effective Masses of Phosphorous Nanoribbons. *Nano Lett.* **14,** 4607−4614 (2014).
13. Wu, M., Qian, X. & Li, J. Tunable Exciton Funnel Using Moiré Superlattice in Twisted van der Waals Bilayer. *Nano Lett.* **14,** 5350−5357 (2014).
14. Buscema, M. *et al.* Fast and Broadband Photoresponse of Few-Layer Black Phosphorus Field-Effect Transistors. *Nano Lett.* **14,** 3347−3352(2014).
15. Tran, V. *et al.* Layer-controlled band gap and anisotropic excitons in few-layer black phosphorus. *Phys. Rev. B* **89,** 235319 (2014)
16. Tran, V. & Yang, L. Scaling laws for the band gap and optical response of phosphorous nanoribbons. *Phys. Rev. B* **89,** 245407 (2014).
17. Rodin, A. S., Carvalho, A. & Castro Neto, A. H. C. Excitons in anisotropic two-dimensional semiconducting crystals. *Phys. Rev. B* **90,** 075429 (2014).
18. Peng, X., Wei, Q. & Copple, A. Strain-engineered direct-indirect band gap transition and its mechanism in two-dimensional phosphorous. *Phys. Rev. B* **90,** 085402 (2014)
19. Lv, H. Y., Lu, W. J., Shao, D. F. & Sun, Y. P. Enhanced thermoelectric performance of phosphorous by strain-induced band convergence. *Phys. Rev. B* **90,** 085433 (2014).
20. Zhu, Z. & Tománek, D. Semiconducting Layered Blue Phosphorus: A Computational Study. *Phys. Rev. Lett.* **112,** 176802 (2014).
21. Guan, J., Zhu, Z. & Tománek, D. Phase Coexistence and Metal-Insulator Transition in Few-Layer Phosphorous: A Computational Study. *Phys. Rev. Lett.* **113,** 046804 (2014).
22. Guo, H. *et al.* Phosphorous Nanoribbons, Phosphorus Nanotubes, and van der Waals Multilayers. *J. Phys. Chem. C* **118,** 14051−14059 (2014).
23. Keyes, R. W. The electrical properties of black phosphorus. *Phys. Rev.* **92,** 580 (1953).
24. Warschauer, D. Electrical and optical properties of crystalline black phosphorus. *J. Appl. Phys.* **34,** 1853 (1963).
25. Qiao, J. *et al.* High-mobility transport anisotropy and linear dichroism in few-layer black phosphorus. *Nat. Commun.* **5,** 4475 (2014).
26. Liang, L. *et al.* Electronic Band gap and Edge Reconstruction in Phosphorene Materials. *Nano Lett.* **14,** 6400−6406 (2014).
27. Wang, X. *et al.* Highly Anisotropic and Robust Exictions in Monolayer Black Phosphorus. arXiv:1411.1695.
28. Akahama, Y., Endo, S. & Narita, S.-I. Electrical properties of black phosphorus single crystals. *J. Phys. Soc. Jpn.* **52,** 2148 (1983).
29. Morita, A. Semiconducting Black Phosphorus. *Appl. Phys. A: Mater. Sci. Process.* **39,** 227 (1986).
30. Zhang, J. *et al.* Phosphorous nanoribbon as a promising candidate for thermoelectric applications. *Sci. Rep.* **4,** 6452 (2014).
31. Wei, Q. & Peng, X. Superior mechanical flexibility of phosphorous and few-layer black phosphorus. *Appl. Phys. Lett.* **104,** 251915 (2014).
32. Liu, H. *et al.* The Effect of Dielectric Capping on Few-Layer Phosphorous Transistors: Tuning the Schottky Barrier Heights. *IEEE Electron Dev. Lett.* **35,** 795–797 (2014).
33. Zhang, S. *et al.* Extraordinary Photoluminescence and Strong Temperature/Angle-Dependent Raman Responses in Few-Layer Phosphorous. *ACS Nano* **8,** 9590–9596 (2014).
34. Deng, Y. *et al.* Black Phosphorus-Monolayer MoS_2 van der Waals Heterojunction p-n Diode. *ACS Nano* **8,** 8292–8299 (2014).
35. Dai J. & Zeng, X. C. Bilayer Phosphorous: Effect of Stacking Order on Bandgap and Its Potential Applications in Thin-Film Solar Cells. *J. Phys. Chem. Lett.* **5,** 1289−1293 (2014).
36. Kou, L., Frauenheim, T. & Chen, C. Phosphorous as a Superior Gas Sensor: Selective Adsorption and Distinct I−V Response. *J. Phys. Chem. Lett.* **5,** 2675−2681 (2014).
37. Rodin, A. S., Carvalho, A. & Castro Neto, A. H. Strain-Induced Gap Modification in Black Phosphorus. *Phys. Rev. Lett.* **112,** 176801 (2014).
38. Zhang, Y., *et al.* Ambipolar MoS_2 Thin Flake Transistors. *Nano Lett.* **12,** 1136−1140 (2012)
39. Shao, Z.-G., Ye, X.-S., Yang, L. & Wang, C.-L. First-principles calculation of intrinsic carrier mobility of silicene. *J. Appl.* **Phys.114,** 093712 (2013).

40. Ye, X.-S. *et al.* Intrinsic carrier mobility of germanene is larger than graphene's: first-principle calculations. *RSC Adv*. **4,** 21216 (2014).
41. Radisavljevic, B.&Kis, A.Mobility engineering and a metal-insulator transition in monolayer MoS_2. *Nat. Mater.* **12,** 815–820 (2013).
42. Momma, K. & Izumi, F. VESTA 3 for three-dimensional visualization of crystal, volumetric and morphology data. *J. Appl. Crystallogr*. **44,** 1272–1276 (2011).
43. Long, M.-Q. *et al.* Theoretical Predictions of Size-Dependent Carrier Mobility and Polarity in Graphene. *J. Am. Chem. Soc.* **131,** 17728–17729 (2009).
44. Bruzzone, S. & Fiori, G. Ab-initio simulations of deformation potentials and electron mobility in chemically modified graphene and two-dimensional hexagonal boron-nitride. *Appl. Phys. Lett.* **99,** 222108 (2011).
45. Xu, B., *et al.* The effect of acoustic phonon scattering on the carrier mobility in the semiconducting zigzag single wall carbon nanotubes. *Appl. Phys. Lett.* **96,** 183108 (2010).
46. Wang, G. Density functional study on the increment of carrier mobility in armchair graphene nanoribbons induced by Stone-Wales defects. *Phys. Chem. Chem. Phys.* **13,** 11939–11945 (2011).
47. Xiao, J. Theoretical Prediction of electronic Structure and Carrier mobility in Single-walled MoS_2 Nanotubes. *Sci. Rep*. **4,** 4327 (2014).
48. Xi, J. *et al.* First-principles prediction of charge mobility in carbon and organic nanomaterials. *Nanoscale* **4,** 4348–4369 (2012).
49. Deng, W.-Q. & W. A. G. III. Predictions of Hole Mobilities in Oligoacene Organic Semiconductors from Quantum Mechanical Calculations. *J. Phys. Chem. B* **108,** 8614–8621 (2004).
50. Bardeen, J. & Shockley, W. Deformation Potentials and Mobilities in Non-Polar Crystals. *Phys. Rev.* **80,** 72−80 (1950).
51. Kresse, G. & Furthmüller, J. Efficiency of ab-initio total energy calculations for metals and semiconductors using a plane-wave basis set. *Comput. Mater. Sci.* **6,** 15–50 (1996).
52. Perdew, J. P., Burke, K. & Ernzerhof, M. Generalized Gradient Approximation Made Simple. *Phys. Rev. Lett.* **77,** 3865–3868(1996).
53. Perdew, J. P., Burke, K. & Ernzerhof, M. Perdew, Burke, and Ernzerhof Reply. *Phys. Rev. Lett.* **80,** 891 (1998).

Acknowledgments

This work is supported by Hunan Key Laboratory for Super-microstructure and Ultrafast Process, and the National Natural Science Foundation of China (Nos. 61306149 and 11334014), the Natural Science Foundation of Hunan Province (No. 14JJ3026), Hong Kong Scholars Program (No. XJ2013003), ShenghuaLieying Scholarship by the Central South University and Hunan Provincial Innovation Foundation for Postgraduate.

Author Contributions

J. X. carried out the first-principles calculations, prepared all figures and wrote the manuscript. M. L. directed this work and revised the manuscript. X. Z., J. O., H. X. and Y. G. involved in discussion. All authors analyzed the results and reviewed the manuscript.

Additional Information

Competing financial interests: The authors declare no competing financial interests.

How to cite this article: Xiao, J. *et al*. Theoretical predictions on the electronic structure and charge carrier mobility in 2D Phosphorus sheets. *Sci. Rep.* **5**, 09961; doi: 10.1038/srep09961 (2015).